Published in final edited form as:
J Am Coll Cardiol. 2010 October 19; 56(17): 1386–1394. doi:10.1016/j.jacc.2010.03.098.

Optical mapping of the isolated coronary-perfused human sinus node

Vadim V. Fedorov, PhD[1], **Alexey V. Glukhov, PhD**[1], **Roger Chang**[1], **Geran Kostecki**[1], **Hyuliya Aferol**[1], **William J. Hucker, MD, PhD**, **Joe Wuskell, PhD**[2], **Leslie M. Loew, PhD**[2], **Richard B. Schuessler, PhD**[3], **Nader Moazami, MD**[3], and **Igor R. Efimov, PhD**[1]

[1]Department of Biomedical Engineering, Washington University, Campus Box 1097, One Brookings Drive, St. Louis, MO, USA

[2]University of Connecticut Health Center, Farmington, CT, USA

[3]Department of Surgery, Washington University School of Medicine, St. Louis, MO, USA

Abstract

Background—The site of origin and pattern of excitation within the human sinoatrial node (SAN) has not been directly mapped.

Objective—We hypothesized that the human SAN is functionally insulated from the surrounding atrial myocardium except for several exit pathways which electrically bridge the nodal tissue and atrial myocardium.

Methods—The SAN was optically mapped in coronary perfused preparations from non-failing human hearts (n=4, age 54±15 years) using dye Di-4-ANBDQBS and Blebbistatin. SAN 3D structure was reconstructed using histology.

Results—Optical recordings from the SAN had diastolic depolarization and multiple upstroke components, which corresponded to the separate excitations of the SAN and atrial layers. Excitation originated in the middle of the SAN (66±17 BPM), then slowly (1–18 cm/s) and anisotropically spread. After a 82±17 ms conduction delay within the SAN, the atrial myocardium was excited via superior, middle, and/or inferior sinoatrial conduction pathways. Atrial excitation was initiated 9.4±4.2 mm from the leading pacemaker site. The oval 14.3±1.5 × 6.7±1.6 × 1.0±0.2 mm SAN structure was functionally insulated from the atrium by connective tissue, fat, and coronary arteries, except for these pathways.

Conclusion—These data demonstrated for the first time the location of the leading SAN pacemaker site, the pattern of excitation within the human SAN, and the conduction pathways into the right atrium. The existence of these pathways explained why, even during normal sinus rhythm, atrial breakthroughs could arise from a region parallel to the CT that is significantly larger (26.0±7.8 mm) than the area of the anatomically defined SAN.

Address for correspondence: Igor R. Efimov, Department of Biomedical Engineering, Washington University, Campus Box 1097, One Brookings Drive, St. Louis, MO, USA. (314) 935-8612, (314) 935-7448 (fax), igor@wustl.edu.

Disclosures: None

Keywords

Human sinoatrial node; optical mapping; exit pathways, atrial breakthrough

INRODUCTION

Despite numerous detailed studies of the origin of excitation in the sinoatrial node (SAN) of many animal species, only excitation of the atrial myocardium and indirect measurements of SAN function have been recorded in humans.(1–3) The major obstacle is the inability of epi- and endocardial electrode mapping to determine the excitation origin and slow propagation of action potentials within the three dimensional (3D) structure of the SAN before it activates the adjacent atrial myocardium.(4–6) Numerous epicardial(7;8) and endocardial(9) mapping studies demonstrated anatomically widespread sites of early atrial activation, which sometimes fire simultaneously. Such multifocal activation started simultaneously during normal sinus rhythm (SR) in humans in 2–5 foci located >1cm apart. The atrial breakthroughs were reported to arise at the epicardial and/or endocardial region along the crista terminalis, over a region 7.5 cm(8;9) in length. That region is significantly larger than the length of the anatomical SAN, which is only 10–18 mm.(10;11) Thus, the origin of excitation and pattern of transmural conduction within the human SAN remain unknown.

Several hypotheses were proposed to explain the relationship between anatomical structure and function of the SAN.(4) The Boineau-Schuessler SAN model(4;12) hypothesized discrete sinoatrial exit pathways (SEP) to explain the multifocal atrial surface activation and shifting site of earliest activation. They hypothesized that depolarization originates and slowly spreads within the SAN and then is transmitted to the atria via several specialized conduction SEPs. We recently presented functional and structural evidence in support of the Boineau-Schuessler hypothesis for the canine SAN, which is anatomically and functionally similar to the human SAN.(5;13) In that study, we developed a new analytical approach which was utilized to resolve the intramural activation pattern of the canine SAN from high resolution optical action potential recordings.(6)

The present study shows for the first time optically mapped coronary perfused intact human atria, including the SAN and nearby atrial myocardium during normal SR. Histology was used to investigate the relationship between function and the 3D anatomic structure of the human SAN.

METHODS

In vitro preparation of the human SAN

Optical mapping studies were conducted in four isolated coronary-perfused preparations of the human SAN similar to our previous study of the human atrioventricular junction.(14) Explanted donor hearts were obtained from Mid-America Transplant Services. Hearts were rejected from transplantation due to age and/or cardiac arrhythmias and were donated for research in accordance with a protocol approved by the Washington University School of Medicine Institutional Review Board. Hearts were cardioplegically arrested in the standard fashion and then were removed with intact superior and inferior vena cavae (SVC and IVC), as shown in Online Figure 1. Hearts were stored in cold cardioplegic solution at 4°C during transport, dissection, and cannulation with a total cold ischemic time of 60–80 minutes. The cardioplegic solution contained (in mM): 110 NaCl, 1.2 $CaCl_2$, 16 KCl, 16 $MgCl_2$, 10 $NaHCO_3$. Online Table 1 presents patient demographics.

The proximal right and left coronary arteries were separately cannulated with custom made polyethylene cannula (ID, 0.86 mm; OD, 1.27 mm). The ventricles were removed and all ventricular branches of the left and right coronary arteries were ligated. The entire atrial preparation was positioned in a temperature-controlled glass chamber with the right atrial (RA) posterior epicardium facing the optical apparatus. The preparation was instrumented with two bipolar pacing and recording electrodes placed on the RA free wall epicardium and the intratrial septum (IAS) (see Online Figure 1). The human atrial preparations were superfused (80 ml/min) and coronary perfused using two pumps (Peri-Star 291, WPI, USA) under a constant pressure of 55±5 mmHg with oxygenated (95%/5%, O_2/CO_2) modified Tyrode's solution containing (in mM): 128.2 NaCl, 1.3 $CaCl_2$, 4.7 KCl, 1.05 $MgCl_2$, 1.19 NaH_2PO_4, 25 $NaHCO_3$, and 11 glucose. Temperature and pH were continuously maintained at 36±0.5°C and 7.35±0.05, respectively.

Experimental protocol

The preparations were equilibrated during SR in the tissue chamber for 60–90 min before the measurements were taken. Blebbistatin (10–20 μM) was perfused to suppress motion artifacts in the optical signals.(15) The preparations were stained with 10–40 μM infrared voltage-sensitive dye di-4-ANBDQBS via coronary perfusion.(16) The SAN preparations were restained by the dye during the experiment as needed. No measurements were performed until 5 min after completing the restaining procedure. Stability of the preparation was periodically verified by measuring SR cycle length (CL).

Fluorescent signals were recorded from the epicardial optical field of view (OFV) ranging in size from 30×30 to 40×40 mm^2 with a spatial resolution of 300–400 μm/pixel at a rate of 1000 frames/s using a 100×100 Ultima-L CMOS camera (SciMedia, Japan). The OFV included portions of the SVC, inferior SAN, crista terminalis (CT) and IAS regions. Programmed atrial stimulation was used to measure atrial conduction properties at different cycle lengths (CL=500–1000 ms).

Optical mapping data analysis and interpretation

A custom Matlab computer program was used to analyze the optical action potentials (OAP) in the SAN and the atria as previously described.(6) Optical recordings contained fluorescent signals from the myocardium up to a depth of 1–3 mm.(16–19) The methodological details of the SAN optical mapping are summarized in a review.(20)

Sinoatrial conduction time (SACT) was the time between the earliest excitation in the SAN and the earliest atrial activation (breakthrough) determined by the second optical upstroke, which represented atrial excitation (Figure 1). Activation times and corresponding conduction velocities (CV) were defined in the SAN layer using 50% of the SAN OAP amplitude (AP50% see Figure 1B).(6;21;22) The atrial layer activation times and pattern were defined by the $-dV/dt_{max}$ of the atrial OAP component (Figure 1B). The conduction Block zone for atrial activation was defined as an area with CV < 20 cm/sec (Figure 1C).

The slope of the slow diastolic depolarization was determined by measuring the slope of a linear fit of diastolic depolarization and normalizing it's amplitude to the OAP amplitude.

Histology

Histology was performed as previously described.(21) After optical mapping experiments, human SAN preparations (n=4) were perfused with 3.7% formaldehyde, frozen in isopentane, cryosectioned perpendicular to the epicardium, and stored at −80°C until staining and imaging was performed (Figures 1D).

RESULTS

Conduction within the SAN

Figure 1 illustrates the functional and anatomical boundaries of the human SAN #1. The SAN region was functionally defined from the morphology of OAPs according to two criteria: presence of a slow diastolic depolarization and upstrokes with multiple components corresponding to activation in different layers of conduction (Figures 1B and 1C, Online Figure 2). The OAPs were then used to reconstruct two separate activation patterns: *slow SAN* excitation from the leading pacemaker (Figure 1C, **left panel**), and *fast atrial* excitation originating from the SEPs (Figure 1C, **middle panel**). S*low SAN* activation patterns near the leading pacemakers were reconstructed in all 4 preparations (Figure 1, Online Figures 3–5). The intranodal activation began in the center of the SAN (OAP #1) and anisotropically spread along the CT, being faster in the inferior and superior directions. Under control conditions, CV within 2–3 mm of the leading pacemaker site (n=4) was 8.7 ± 3.8 cm/s and 6.5 ± 1.3 cm/s in the superior and inferior directions, respectively; 6.1 ± 5.3 cm/s in the lateral direction toward the CT; and 3.5 ± 2.6 cm/s ($p<0.05$ vs. superior CV) medially toward the septum, with a maximum anisotropy CV ratio of 3.3±1.9.

Due to epicardial fibrosis and fat above the SAN, optically-detected SAN areas were less than anatomical projections of the node on the epicardium: length 6.8±1.0 mm vs 14.3 ±1.5 mm and width 4.8±0.5 mm vs 6.3±1.5 mm, respectively. These anatomical features prevented complete reconstruction of the activation pattern between the SAN and atrial myocardium.

Atrial breakthrough sites

The sites of earliest epicardial activation of the atrial working myocardium were defined as atrial breakthrough sites. In Figure 1, the breakthrough site (OAP #2), was detected 75 ms after the earliest SAN activation and located 5 mm superior and lateral to the site of the earliest SAN activation. On average, atrial breakthrough during control conditions occurred 82±17 ms (SACT) after the earliest SAN activation and theses sites were located 9.4±4.2 mm superior or inferior to the site of the earliest activation within the SAN. Following the breakthrough, atrial activation rapidly spread along the CT (120–140 cm/sec) and through the RA free wall (70–90 cm/sec), but slowly spread toward the IAS (OAP #3). Histology sections showed that the block area coincided with the septal margin of the SAN, which was separated from atrial myocardial bundles in the IAS and CT by connective tissue, fat, and coronary arteries.

During SR, two preparations (#1 and #3) had a superior breakthrough site, one (#2) had two breakthrough sites, and one (#4) had an inferior breakthrough site (Figure 1, Online Figures 3–5).

The sites of the leading pacemaker in the SAN and atrial breakthrough remained stable for about 1–2 hours during experiments. At the beginning of each experiment, after the stabilization period (60–90 minutes), the SR CL ranged from 651 ms to 1120 ms. However, during the course of the experiment the SR CL slowed from 951±206 ms to 1159±346 ms. As the SR CL slowed, the site of the atrial breakthrough(s) could abruptly shift inferiorly toward the IVC. Atrial breakthrough sites also could be transiently shifted by overdrive atrial pacing.

Effects of atrial pacing on SAN conduction

Following 1–10 minutes of overdrive atrial pacing, the superior atrial breakthrough shifted inferiorly and/or multifocal breakthroughs were observed (Figure 2). Figure 2 shows the

dynamic changes of the SAN and atrial activation patterns, which were recorded in preparation #1 before (**panel A**) and after 5 minutes (**panel B**) of atrial pacing at the start of the experiment, and two hours later (**panel C**). Before pacing, the atrial activation pattern was unifocal, originating from the superior SEP (SACT=78 ms) (Figure 2A). Atrial pacing slowed conduction in the superior part of the SAN and the pacemaker shifted 1 mm superior (Figure 2B). Excitation then propagated through the lateral SEP faster than the superior SEP, resulting in a bifocal initiation of atrial activation with no significant change in SACT (80 ms). Bifocal breakthroughs abruptly switched to superior unifocal breakthroughs less than one minute after pacing was stopped.

However, after two hours, both the superior and lateral SEPs failed to conduct and inferior unifocal atrial breakthrough occurred (Figure 2C). Atrial pacing induced significant slowing of SR and a two-fold slowing of SAN conduction velocity, as well as a 2 mm inferior shift of the earliest pacemaker. SAN excitation slowly propagated through the inferior SEP and reached the atria after a 157 ms delay, 15 mm inferior to the site of the earliest activation within the SAN. CV could not be directly measured within the SEPs due to the poor quality of signals. However, the CV could be estimated by dividing the distance between SAN activation and atrial breakthrough sites by the time difference, yielding a SEP CV of 3–12 cm/sec.

Long coronary perfusion of the human atria resulted in slowing of both SR CL and SAN conduction delay, which could extend to more than 400 ms. Figure 3 shows such an example of the pacing induced conduction block (slowing) after 3 hours of perfusion. After 5 minutes of atrial pacing (CL=1000 ms), the OAP tracings from the leading pacemaker area (Figure 3A, OAP #1) demonstrated slow, small amplitude signals, reflecting only SAN action potentials. SAN excitation originated near the same leading pacemaker site as observed prior to pacing, but was blocked in the superior SEP and slowly propagated at 3.7 cm/sec through the inferior SEP.

In all SAN preparations (n=4), epicardial optical mapping revealed at least three main atrial breakthrough sites, which corresponded to the superior, lateral, and inferior SEPs, with a maximum distance between them of 26.1±7.9 mm (Figure 4).

Relating SAN function to structure

Figure 4 shows a combination of functional and structural characteristics of the human SAN #1. The left panels were two views of a single preparation, and included anatomical annotations. From nearly 300 Mason-Trichome histology sections of a single human heart, 23 histology images at different depths were chosen to represent the structural features of the human SAN. In each of the selected histology images (right panel), various anatomical features were manually identified and drawn using Rhinoceros software (McNeel, Seattle, WA), as previously described.(23) The anatomical regions included were the SAN, coronary arteries, fibrous tissue, fat, and the surrounding atrial tissue. The SAN was identified in the histology images as the dense fibrotic and cardiomyocyte compact region near the epicardium. Dotted outlines of the SAN and coronary arteries between the histology images in the right panel depicted the structures of these two features throughout the SAN region.

Volume rendering of the anatomical features in the human heart sample was formed by connecting all of the tracings in each of the sections. Combining these volume renderings of individual anatomic structured into one model (Figure 5) allowed the functional observations to be related to the anatomical features surrounding the SAN. Of note:

1. The double-component SAN OAPs only occurred in the structural SAN region.
2. The fibrotic tissue and fat layers were significant conduction barriers.

3. The SAN activation pattern and the sites of atrial breakthroughs allowed tracking of the SEPs.
4. Fat and fibrotic layers > 1 mm thick between the SAN tissue and the epicardium diminished the SAN component.

DISCUSSION

Structural and functional characteristics of the human SAN

This study used optical mapping to show for the first time the location of the leading pacemaker and the conduction pattern within and near the SAN during normal sinus rhythm. The human SAN is a complex 3D structure that is anatomically and functionally isolated from the atrial myocardium (CT and IAS) except for several SEPs (Figure 5). Functionally, excitation of the SAN precedes the earliest excitation of the atrial myocardium by 82±17 ms. SAN excitation is then transmitted from the SAN via superior, lateral and/or inferior SEPs which are located 9.4±4.2 mm from the leading pacemaker site.

These observations support the Boineau-Schuessler hypothetical model of the SAN(4;12) and are in agreement with our prior report on the canine SAN.(6) Previous histological and immonohistochemical studies by James,(10;13;24) Truex et al.,(11;25) and Schuessler et al. (5;26) support our functional and structural data, which demonstrate that the canine and human SAN are electrically insulated from most of the nearby atrial myocardium except for several SEPs. This conduction barrier is formed by the sinus nodal coronary arteries, connective tissue, and fat, as well as an abrupt change in Cx43 expression between atrial and nodal cells.(6;27)

While the present study observed unifocal activation in the SAN, there were bifocal breakthroughs in the atrial myocardium (Figure 2). Atrial overdrive pacing could slow SAN pacemaker activity and conduction within the SAN, both of which shifts the pacemaker 1–2 mm within the node. The pacemaker shift caused excitation through a different SEP and activated the atria at inferior breakthrough site. Figure 3 shows an example of a 2 mm pacemaker shift, which resulted in a 20 mm breakthrough site caudal shift. During normal SR, multifocal initiation of atrial activation did not originate from multiple simultaneous pacemakers, but rather corresponded to a single leading pacemaker site within the SAN that simultaneously excited the atrium via multiple SEPs (Figure 4). Under other conditions, however, it is possible that subsidiary pacemakers outside the SAN could cause a multifocal initiation of multifocal breakthroughs in the atrium.

The present study provides direct intranodal measurements of CVs within 2–3 mm of the leading pacemaker site in the four human preparations, CV= 0.9–14 cm/s (Figure 1, Online Figures 3–5). These values are in agreement with those seen in other mammalian species. (2;6;21;28;29) However, in the rabbit and other small mammals, the propagating wide wavefront moves from the leading pacemaker at an accelerating speed directly toward the CT.(21) In contrast, in the canine(6) and human SAN, the propagating wavefront slows down before and within channel(s) of SEP which are utilized to excite the atrial myocardium. It is likely that conduction in these pathways slows down due to a source-sink mismatch. A weak source of current in the narrow exit pathway must excite the large load of the hyperpolarized funnel-like expansion of the atrial muscle. A similar behavior was studied in detail in 2D cell culture structures.(30) We hypothesize that due to the 3D nature of the SAN of large mammals, the node must be more electrically insulated from the surrounding 3D atrial myocardium as compared to small mammals, which have 2D SAN and thin atrial myocardium.

Study Limitations

Diversity of the donor history (age, arrhythmias, low ejection fraction, hypertrophy and drugs) could affect the present results. Rejected donor hearts are not physiologically normal and are denervated, and therefore findings from this study cannot be fully extrapolated to normal healthy human hearts.

Duration of in vitro optical recordings was limited due to washout and/or photobleaching of the dye, and edema.(6;31) We used Blebbistatin, which had been successfully applied in rat and rabbit,(15) canine(6) and human heart models.(14) However, it is possible that suppression of mechanical contractions by Blebbistatin prevented activation of stretch-sensitive channels, which can play a role in pacemaker activity in the SAN.(32)

Our direct measurements of SACT (82±17 ms) and right atrial CVs (70–160 cm/sec) correlated well with clinical data,(33–36) which suggests that the perfused preparations were well preserved.

We cannot exclude the potential influence of edema that may develop in a mechanically silent preparation and may affect SAN pacemaker and conduction properties.

Optical resolution is limited by the point-spread function in tissue, which is 500–1000 μm and further restricted by scattering in epicardial fat and connective tissue in the SAN region. Therefore, we could not map the entire SAN and all exit pathways in some hearts. However, consistency of signal morphology in the SAN region, i.e. SAN component preceding atrial component, indicates that we had conduction between the SAN and atrium via an exit pathway.

CONCLUSION

These data demonstrate for the first time the location of the leading pacemaker and the conduction pattern within and near the intact human sinus node. The present study demonstrates functional insulation of the human sinus node from the atria, except for multiple SEPs. These pathways are important in the modulation of sinus rhythm and atrial activation patterns. The presence of multiple SEPs explained the occurrence of multiple atrial breakthroughs arising during normal SR from a region significantly larger than the area of the anatomical SAN (26.1±7.9 mm) parallel to the CT.

Supplementary Material

Refer to Web version on PubMed Central for supplementary material.

Acknowledgments

The project was supported by the AHA BGIA 0860047Z (VVF), NIH R01 HL085369 (IRE), NIH R01 HL 032257(RBS) and NIH R01 HL085113 (RBS).

Reference List

1. Boyett MR, Honjo H, Kodama I. The sinoatrial node, a heterogeneous pacemaker structure. Cardiovasc Res. 2000; 47:658–687. [PubMed: 10974216]
2. Opthof T, de Jonge B, Jongsma HJ, et al. Functional morphology of the mammalian sinuatrial node. Eur Heart J. 1987; 8:1249–1259. [PubMed: 3691562]
3. Verkerk AO, van Ginneken AC, Wilders R. Pacemaker activity of the human sinoatrial node: role of the hyperpolarization-activated current, I(f). Int J Cardiol. 2009; 132:318–336. [PubMed: 19181406]

4. Schuessler RB. Abnormal sinus node function in clinical arrhythmias. J Cardiovasc Electrophysiol. 2003; 14:215–217. [PubMed: 12693509]
5. Bromberg BI, Hand DE, Schuessler RB, et al. Primary negativity does not predict dominant pacemaker location: implications for sinoatrial conduction. Am J Physiol. 1995; 269:H877–H887. [PubMed: 7573531]
6. Fedorov VV, Schuessler RB, Hemphill M, et al. Structural and functional evidence for discrete exit pathways that connect the canine sinoatrial node and atria. Circ Res. 2009; 104:915–923. [PubMed: 19246679]
7. Durrer D, Dam RTv, Freud GE, et al. Total excitation of the isolated human heart. Circulation. 1970; 41:899–912. [PubMed: 5482907]
8. Boineau JP, Canavan TE, Schuessler RB, et al. Demonstration of a widely distributed atrial pacemaker complex in the human heart. Circulation. 1988; 77:1221–1237. [PubMed: 3370764]
9. Cosio FG, Martin-Penato A, Pastor A, et al. Atrial activation mapping in sinus rhythm in the clinical electrophysiology laboratory: observations during Bachmann's bundle block. J Cardiovasc Electrophysiol. 2004; 15:524–531. [PubMed: 15149420]
10. James TN. Anatomy of the human sinus node. Anat Rec. 1961; 141:109–139. [PubMed: 14451023]
11. Truex RC, Smythe MQ, Taylor MJ. Reconstruction of the human sinoatrial node. Anat Rec. 1967; 159:371–378. [PubMed: 5586287]
12. Boineau JP, Schuessler RB, Mooney CR, et al. Multicentric origin of the atrial depolarization wave: the pacemaker complex. Circulation. 1978; 58:1036–1048. [PubMed: 709760]
13. James TN. Anatomy of the sinus node of the dog. Anat Rec. 1962; 143:251–265. [PubMed: 14451024]
14. Hucker WJ, Fedorov VV, Foyil KV, et al. Images in cardiovascular medicine. Optical mapping of the human atrioventricular junction. Circulation. 2008; 117:1474–1477. [PubMed: 18347223]
15. Fedorov VV, Lozinsky IT, Sosunov EA, et al. Application of blebbistatin as an excitation-contraction uncoupler for electrophysiologic study of rat and rabbit hearts. Heart Rhythm. 2007; 4:619–626. [PubMed: 17467631]
16. Matiukas A, Mitrea BG, Qin M, et al. Near-infrared voltage-sensitive fluorescent dyes optimized for optical mapping in blood-perfused myocardium. Heart Rhythm. 2007; 4:1441–1451. [PubMed: 17954405]
17. Nikolski V, Efimov I. Fluorescent imaging of a dual-pathway atrioventricular-nodal conduction system. Circ Res. 2001; 88:E23–E30. [PubMed: 11179207]
18. Baxter WT, Mironov SF, Zaitsev AV, et al. Visualizing excitation waves inside cardiac muscle using transillumination. Biophys J. 2001; 80:516–530. [PubMed: 11159422]
19. Efimov IR, Mazgalev TN. High-resolution three-dimensional fluorescent imaging reveals multilayer conduction pattern in the atrioventricular node. Circulation. 1998; 98:54–57. [PubMed: 9665060]
20. Efimov IR, Fedorov VV, Joung B, et al. Mapping cardiac pacemaker circuits: methodological puzzles of the sinoatrial node optical mapping. Circ Res. 2010; 106:255–271. [PubMed: 20133911]
21. Fedorov VV, Hucker WJ, Dobrzynski H, et al. Postganglionic nerve stimulation induces temporal inhibition of excitability in the rabbit sinoatrial node. Am J Physiol. 2006; 291:H612–H623.
22. Fedorov VV, Hepmpill M, Kostecki G, et al. Low electroporation threshold, conduction block, focal activity and reentrant arrhythmia in the rabbit atria: possible mechanisms of stunning and defibrillation failure. Heart Rhythm. 2008; 5:593–604. [PubMed: 18362029]
23. Hucker WJ, McCain ML, Laughner JI, et al. Connexin 43 expression delineates two discrete pathways in the human atrioventricular junction. Anat Rec (Hoboken). 2008; 291:204–215. [PubMed: 18085635]
24. James TN. Structure and function of the sinus node, AV node and His bundle of the human heart: part I-structure. Prog Cardiovasc Dis. 2002; 45:235–267. [PubMed: 12525999]
25. Truex RC, Smythe MQ. Comparative morphology of the cardiac conduction tissue in animals. Ann N Y Acad Sci. 1965; 127:19–33. [PubMed: 5217260]

26. Kwong KF, Schuessler RB, Green KG, et al. Differential expression of gap junction proteins in the canine sinus node. Circ Res. 1998; 82:604–612. [PubMed: 9529165]
27. Chandler NJ, Greener ID, Tellez JO, et al. Molecular architecture of the human sinus node: insights into the function of the cardiac pacemaker. Circulation. 2009; 119:1562–1575. [PubMed: 19289639]
28. Sano T, Yamagishi S. Spread of excitation from the sinus node. Circ Res. 1965; 16:423–430. [PubMed: 14289151]
29. Bleeker WK, Mackaay AJ, Masson-Pevet M, et al. Asymmetry of the sinoatrial conduction in the rabbit heart. J Mol Cell Cardiol. 1982; 14:633–643. [PubMed: 7154097]
30. Rohr S, Kucera JP, Fast VG, et al. Paradoxical Improvement of Impulse Conduction in Cardiac Tissue by Partial Cellular Uncoupling. Science. 1997; 275:841–844. [PubMed: 9012353]
31. Efimov IR, Nikolski VP, Salama G. Optical imaging of the heart. Circ Res. 2004; 95:21–33. [PubMed: 15242982]
32. Cooper PJ, Kohl P. Species- and preparation-dependence of stretch effects on sino-atrial node pacemaking. Ann N Y Acad Sci. 2005; 1047:324–335. [PubMed: 16093508]
33. Hadian D, Zipes DP, Olgin JE, et al. Short-term rapid atrial pacing produces electrical remodeling of sinus node function in humans. J Cardiovasc Electrophysiol. 2002; 13:584–586. [PubMed: 12108502]
34. Gomes JA, Kang PS, El Sherif N. The sinus node electrogram in patients with and without sick sinus syndrome: techniques and correlation between directly measured and indirectly estimated sinoatrial conduction time. Circulation. 1982; 66:864–873. [PubMed: 7116602]
35. Hansson A, Holm M, Blomstrom P, et al. Right atrial free wall conduction velocity and degree of anisotropy in patients with stable sinus rhythm studied during open heart surgery. Eur Heart J. 1998; 19:293–300. [PubMed: 9519324]
36. Sanders P, Morton JB, Kistler PM, et al. Electrophysiological and electroanatomic characterization of the atria in sinus node disease: evidence of diffuse atrial remodeling. Circulation. 2004; 109:1514–1522. [PubMed: 15007004]

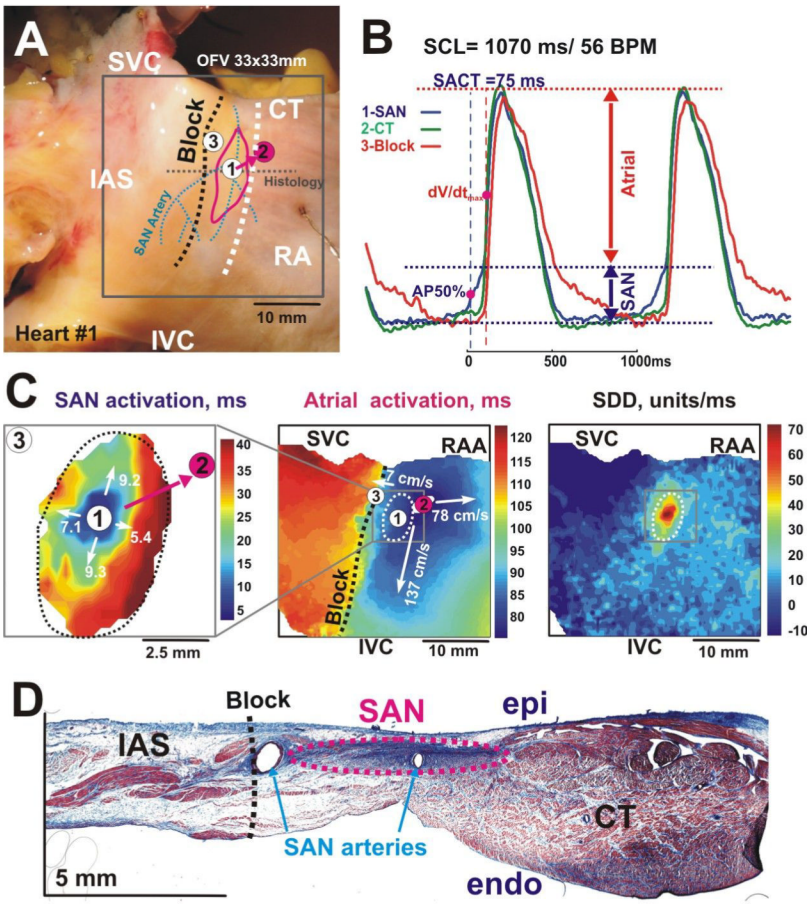

Figure 1. Epicardial optical mapping of the human right atrial preparation #1

Panel A - Epicardial photographs of a perfused human atrial preparation with a 33×33 mm optical field of view (OFV). The pink circle shows superior atrial breakthrough and white circles show all other breakthroughs recorded by optical mapping (see **panel C**, and Figure 4). The SAN arteries are shown by blue dotted lines. The white dashed line shows the location of the sulcus terminalis, which is the medial epicardial edge of the crista terminalis (CT). The red oval shows the approximate border of the SAN region. In all panels, the black dashed line shows the location of the IAS block zone (Block).

Panel B Optical action potentials from the center of the SAN (1), the atrial breakthrough in CT (2), and Block area (3) from sites 1 –3 in **panels A** and **C** during normal SR. Optical recordings show the complex morphology that reflects electrical activity from multiple layers of the tissue, including slowly rising upstrokes of the SAN (SAN component) and rapidly rising upstrokes of the atrial myocardium (Atrial component) above the SAN layer.

Panel C – Separated SAN and atrial activation maps, and slow diastolic depolarization (SDD) map. The grey squares on the Atrial and SDD maps show the SAN region that was mapped. White numbers with arrows show values of the conduction velocities in these directions.

Panel D - This panel shows a single transmural histology section from the center part of the SAN.

Abbreviations: SVC and IVC, superior and inferior vena cava; RAA, right atrial appendage; IAS, intra-atrial septum, SCL, sinus cycle length; SACT, sino-atrial conduction time, AP50% – 50% of the amplitude of the SAN component, dV/dt_{max} – maximum derivative of the atrial upstroke.

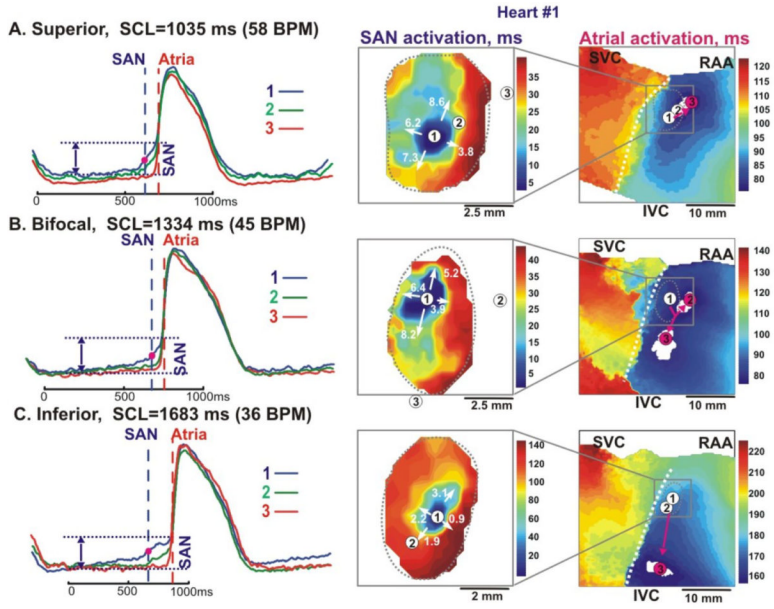

Figure 2. Optical mapping of the SAN excitation during superior, bifocal and inferior atrial breakthrough pattern (heart #1)

The Panels A, B and C, left – Optical action potentials recorded from sites 1–3 on the activation maps, respectively. These optical potentials were recorded before and after atrial pacing for 5–10 min. Vertical dashed lines show the beginning of SAN and Atrial activations, respectively.

The Panels A, B and C, middle and right - Activation maps of the SAN and atrial components, during superior, bifocal and inferior atrial breakthrough patterns, respectively. In all panels, the pink circles show sites of atrial breakthrough; the pink arrows represent the sinoatrial pathways from the SAN to the CT.

Abbreviations are the same as in Figure 1.

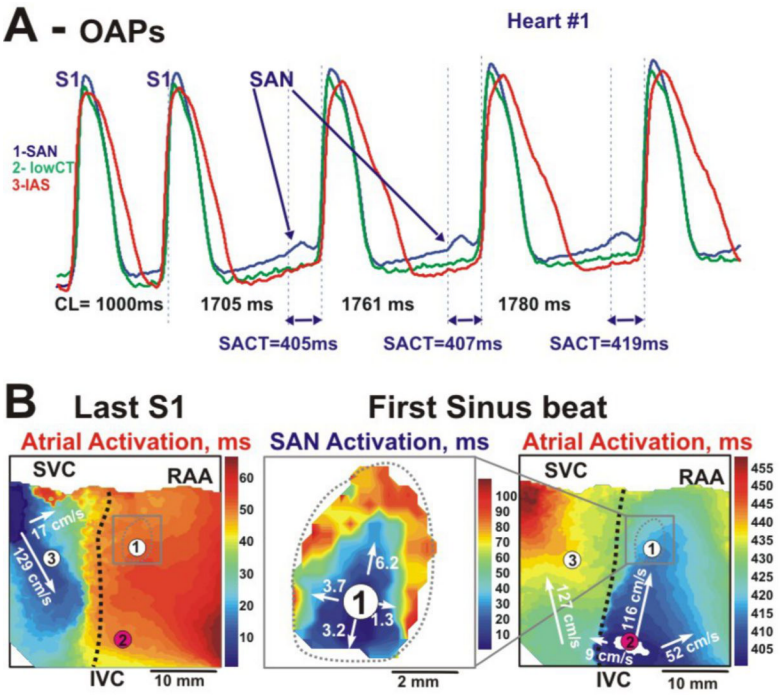

Figure 3. Pacing-induced depression SAN conduction and shift of atrial breakthrough (heart #1)

Panel A - Optical action potentials recorded from three sites depicted in the activation maps (**panel B**) following the termination of atrial pacing with an S1S1=1000 ms and recovery of spontaneous SAN activity. Recordings from the SAN region demonstrate a slow activation (**panel B, middle**) from the pacemaker layer more then 400 ms before the atrial component. **Panel B** - Activation maps during atrial pacing and the first spontaneous SAN excitation after termination of pacing. The first SAN excitation mapped after termination of pacing showed slow propagation, with an average conduction velocity of 3.8 cm/s from the cranial and caudal ends of the SAN. This activation excited the atrial myocardium about 16 mm below the leading pacemaker. The black dotted line shows conduction block to the IAS, which was observed during both pacing and spontaneous excitation. See text for details. Abbreviations are the same as in Figure 1.

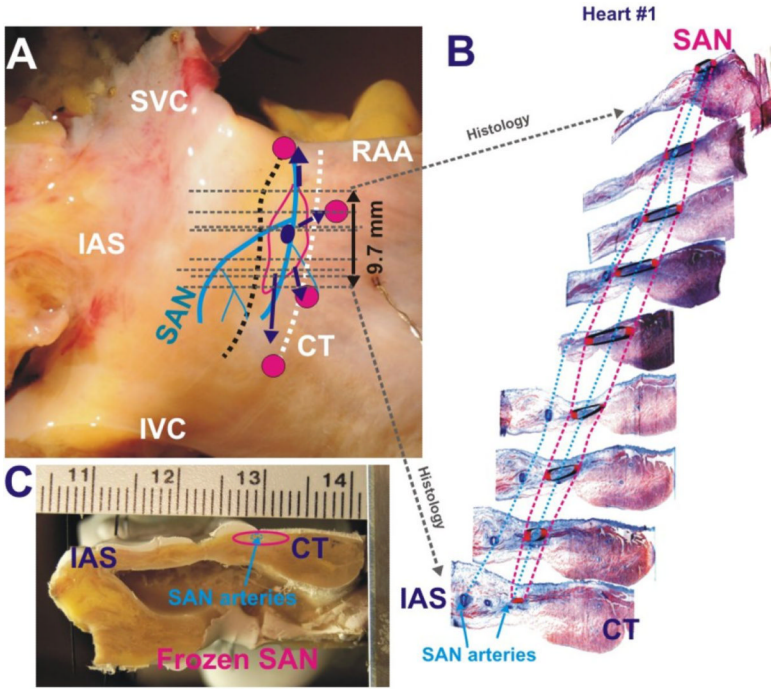

Figure 4. Functional and structural features of the human SAN #1

Panels A and C - Two perpendicular perspectives of the human SAN preparation (#1) including anatomical (arteries – blue lines, SAN – red outline) and functional (SEPs – purple arrows, leading pacemaker site – purple dot, breakthrough sites – magenta dots) features. Grey dashed lines represent location of histology sections shown in Panel B and had the same perpendicular orientation as in Panel C.

Panel B - A series of representative histology slide images that trace the locations of the arteries (blue) and the SAN (red) from superior to inferior ends of the SAN.

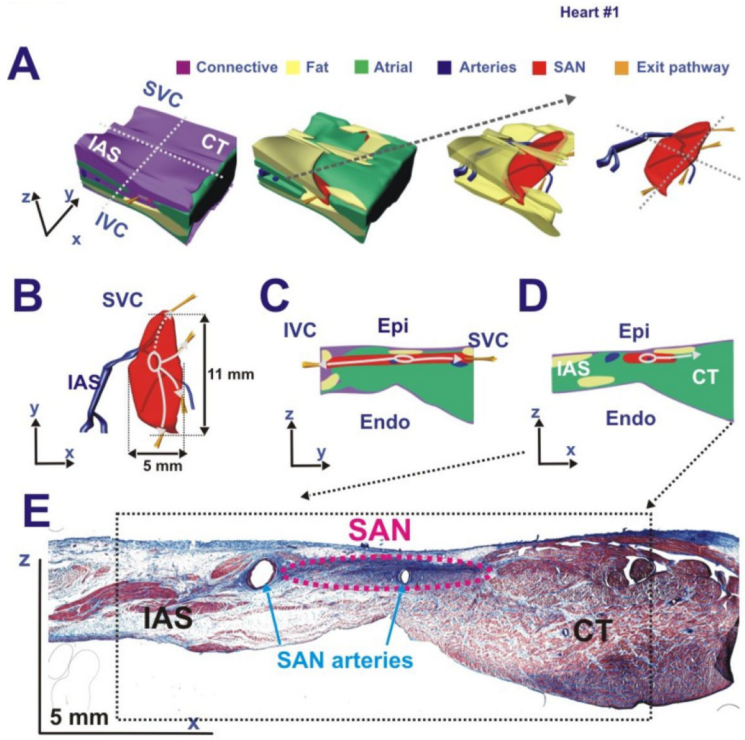

Figure 5. Anatomical 3D model of the human SAN #1

The anatomical features (fibrotic tissue – purple; fat – yellow; green – atrial; SAN – red) in the series of 20 perpendicular histology sections seen in Figure 4 were outlined and Rhinoceros software was used to reconstruct a 3D model of the human SAN #1. This model related the structural features with the functional observations (SEP – gold pathways, leading pacemaker excitation – white oval and arrows). **Panel A** – A collection of side projection images, which displays the multiple layers surrounding the human SAN. **Panel B** – Top epicardial projections of the SAN tissues with arteries and SEPs. **Panels C and D** – Cross-sections in the zy- and zx-planes respectively. **Panel E** –Histology image of the zx-plane view in **Panel D**.